3242 *Chem. Mater.* **2009,** *21,* 3242–3250
DOI:10.1021/cm900767m

CHEMISTRY OF MATERIALS
Article

Topotactic Transformation of the Cationic Conductor $Li_4Mo_5O_{17}$ into a Rock Salt Type Oxide $Li_{12}Mo_5O_{17}$

N. Pop,[†] V. Pralong,*[,†] V. Caignaert,[†] J. F. Colin,[†] S. Malo,[†] G. Van Tendeloo,[‡] and B. Raveau[†]

[†]*Laboratoire CRISMAT, UMR 6508 CNRS ENSICAEN, 6 bd Maréchal Juin, 14050 CAEN, France, and* [‡]*EMAT, University of Antwerp, Groenenborgerlaan 171, B-2020 Antwerp, Belgium*

Received March 19, 2009. Revised Manuscript Received June 2, 2009

Intercalation of lithium in the ribbon structure $Li_4Mo_5O_{17}$ has been achieved, using both electrochemistry and soft chemistry. The ab initio structure determination of the "Mo−O" framework of $Li_{12}Mo_5O_{17}$ shows that the $[Mo_5O_{17}]_\infty$ ribbons keep the same arrangement of edge sharing MoO_6 octahedra and the same orientation as in the parent structure but that a topotactic antidistortion of the ribbons appears, as a result of the larger size of Mo^{4+} in "Li_{12}" compared to Mo^{6+} in "Li_4". On the basis of bond valence calculations, it is observed that 12 octahedral sites are available for Li^+ in the new structure so that an ordered hypothetical rock salt type structure can be proposed for $Li_{12}Mo_5O_{17}$. After the first Li insertion, a stable reversible capacity of 100 mA·h/g is maintained after 20 cycles. A complete structural reversibility leading back to the ribbon type $Li_4Mo_5O_{17}$ structure is obtained using a very low rate of C/100. The exploration of the Li mobility in those oxides shows that $Li_4Mo_5O_{17}$ is a cationic conductor with $\sigma = 10^{-3.5}$ S/cm at 500 °C and $E_a = 0.35$ eV.

Introduction

Electrochemical intercalation of lithium in transition metal oxides has attracted considerable attention these last decades because of the potential of the involved reactions for the realization of Li-ions batteries.[1,2] Thus, a great deal of work has been carried out in this field on various families of oxides—cobalt, manganese, nickel, vanadium, tungsten, titanium, niobium, and molybdenum—whose redox potential values are in adequation with such applications. In most of these studies, the parent structure selected for the electrochemical intercalation is either bidimensionnal or three-dimensional with cages or tunnels allowing a reversible intercalation of lithium without any drastic modification of the structure.[3−6]

To discover new materials, susceptible of potential electrochemical properties, the research of Li-rich compounds (keeping in mind the structural aspects) is of great interest to understand the mechanisms which govern the Li intercalation/deintercalation in such systems.

In this respect, the Li−Mo−O system is very attractive as a result of the ability of molybdenum to adopt various oxidation states and coordinations, to the values of the redox potentials of 2.4 V and 1.6 V for the couples Mo^{6+}/Mo^{5+} and Mo^{5+}/Mo^{4+}, respectively, and to the benign environmental properties of molybdenum oxides. For these reasons, the intercalation of lithium in MoO_3 was studied by several authors, showing its potential as electrochromic [7,8] and cathode materials.[9−14] In contrast, very few lithium molybdenum oxides of the Li−Mo−O system were investigated in view of Li intercalation or deintercalation. In this system, three oxides were studied, namely, the Mo(IV) oxides Li_2MoO_3 [15−17] and $Li_4Mo_5O_{12}$ [15] and the bronzes Li_xMoO_3.[11] The first one was shown to exhibit an interesting cycling capacity of 150 mA·h/g after 10 cycles between 1.5 and 4.3 V, whereas the second one can intercalate $3Li^+$ per f.u.,

*Corresponding author. E-mail: valerie.pralong@ensicaen.fr. Fax: +33 2 31 95 16 00. Tel: +33 2 31 45 26 32.

(1) Poizot, P.; Laruelle, S.; Grugeon, S.; Dupont, L.; Tarascon, J.-M. *Nature* **2000**, *407*, 496.
(2) Armand, M.; Tarascon, J.-M. *Nature* **2008**, *451*, 652.
(3) Bruce, P. G.; Scrosati, B.; Tarascon, J.-M. *Angew. Chem., Int. Ed.* **2008**, *47*, 2.
(4) Whittingham, M. S. *Chem. Rev.* **2004**, *104*, 4271.
(5) Leyzerovich, N. N.; Bramnik, K. G.; Buhrmester, T.; Ehrenberg, H.; Fuess, H. *J.Power Source* **2004**, *127*, 76.
(6) Sharma, N.; Shaju, K. M.; Subba Rao, G. V.; Chowdari, B. V. R.; Dong, Z. L.; White, T. J. *Chem. Mater.* **2004**, *16*, 504.
(7) Dillon, A. C.; Mahan, A. H.; Deshpande, R.; Parilla, P. A.; Jones, K. M.; Lee, S.-H. *Thin Solid Films* **2008**, *516*, 794.
(8) Sivakumar, R.; Manisankar, P.; Jayachandran, M.; Sanjeeviraja, C. *Sol. Energy Mater. Sol. Cells* **2006**, *90*, 2438.
(9) Martinez-de la Cruz, A; Suarez Ramirez, I. *J. Power Sources* **2004**, *133*, 268.
(10) Song, J.; Wang, X.; Ni, X.; Zheng, H.; Zhang, Z.; Ji, M.; Shen, T.; Wang, X. *Mater. Res. Bull.* **2005**, *40*, 1751.
(11) Leroux, F.; Nazar, L. F. *Solid State Ionics* **2000**, *133*, 37.
(12) Kim, S. S.; Ogura, S.; Ikuta, H.; Uchimoto, Y.; Wakihara, M. *Solid State Ionics* **2002**, *146*, 249.
(13) Kobayashi, H.; Tabuchi, M.; Shikano, M.; Nishimura, Y.; Kageyama, H.; Ishida, T.; Nakamura, H.; Kurioka, Y.; Kanno, R. *J. Power Sources* **1999**, *81−82*, 524.
(14) Schollhorn, R.; Kuhlmann, R.; Besenhard, J. O. *Mater. Res. Bull.* **1976**, *11*, 83.
(15) Huang, C.-K.; Crouch-Baker, S.; Huggins, R. A. *J. Electrochem. Soc.* **1988**, *135*, 408.
(16) Tsumura, T.; Inagaki, M. *Solid State Ionics* **1997**, *104*, 183.
(17) James, A. C. W. P.; Goodenough, J. B. *J. Solid State Chem.* **1988**, *76*, 87.

 Published on Web 06/24/2009

corresponding to 123 mA·h/g within a 0.5−2.5 V potential range.[16] The great interest of the bronze $Li_{0.25}MoO_3$ as anode material (low potential) was demonstrated by its retention capacity of 600 mA·h/g after 100 cycles.[11]

Curiously, lithium molybdate Mo(VI) was investigated neither for ionic conductivity nor for the electrochemical Li intercalation viewpoint, in spite of the existence of several phases such as $Li_4Mo_5O_{17}$,[18,19] Li_2MoO_4,[19] and $Li_2Mo_4O_{13}$.[19−22] Bearing in mind the ribbon structure of $Li_4Mo_5O_{17}$, we have explored the ionic conductivity of this phase and its ability to intercalate lithium. In the present paper, we show that $Li_4Mo_5O_{17}$ is a cationic conductor and that it can intercalate up to eight lithium ions per formula unit, according to a reversible topotactic reaction, leading to an ordered rock salt type structure $Li_{12}Mo_5O_{17}$.

Experimental Section

Synthesis of the Precursor $Li_4Mo_5O_{17}$. The parent phase $Li_4Mo_5O_{17}$ was prepared via sol−gel method. MoO_3 (Cerac 99.95%) was dissolved in a solution mixture of 28% NH_3 aqueous and 35% H_2O_2 at low temperature between 5−10 °C. Li_2CO_3 (Aldrich, 99%) was dissolved in diluted HNO_3 and transferred into the molybdenum solution under magnetic stirring at room temperature. Citric acid monohydrate (Prolabo, 99%, molar ratio of citric acid to metal ion was 3:1) and ethylene glycol (Aldrich 99%, molar ratio of ethylene glycol to citric acid was 1:1) were added to the solution. The solution was stirred at 50 °C for 24 h, and the formation of a viscous blue gel was observed. The gel was heated at 300 °C for 1 h, to generate a partial decomposition of organic compounds and formation of a foamy brown precursor. The final compound was obtained by heating the foamy brown precursor at 500 °C for 24 h with intermediate grindings. The average size of the agglomerated particles is 10 μm size. The X-ray powder diffraction pattern showed the formation of pure $Li_4Mo_5O_{17}$ phase, which was refined by the Rietveld method. The refined lattice parameters are in a good agreement with the previous reports.[19] The thermogravimetric study (not shown) revealed that this phase is stable up to 500 °C.

Electrochemical Synthesis and Characterizations. The electrochemistry characterization of $Li_4Mo_5O_{17}$ was performed in Swagelok cells. The negative electrode metallic Li (Aldrich, 99.9%), LP30 from Merck (1 M $LiPF_6$ in an ethylene carbonate (EC)/dimethyl carbonate(DC) 1:1 w/w Selectipur) was used as electrolyte, and the positive electrode was constituted of approximately 10 mg of a mixture of the active material with 30% carbon (acetylene black). The electrochemical cells were cycled at constant current between 2.0 and 3.0 V at different galvanostatic rates on a VMP II potentiostat/galvanostat (Biologic SA, Claix, France) at room temperature. Galvanostatic intermittent titration technique (GITT) measurements consisting of 2 h discharge at C/50 with open circuit periods of 1 h were performed. Potentiostatic intermittent titration technique (PITT)[23,24] measurements were conducted using potential steps of 10 mV limited by a minimum current equivalent to a C/20 galvanostatic rate. Impedance measurements were carried out with an EG&G 7220 lock-in amplifier in the frequency range 10 Hz−120 kHz. Pellets were prepared by cold pressing the powder sample. Gold electrodes were deposited by vacuum evaporation. The impedance measurements were carried out at steady state temperatures from room temperature to 500 °C under vacuum.

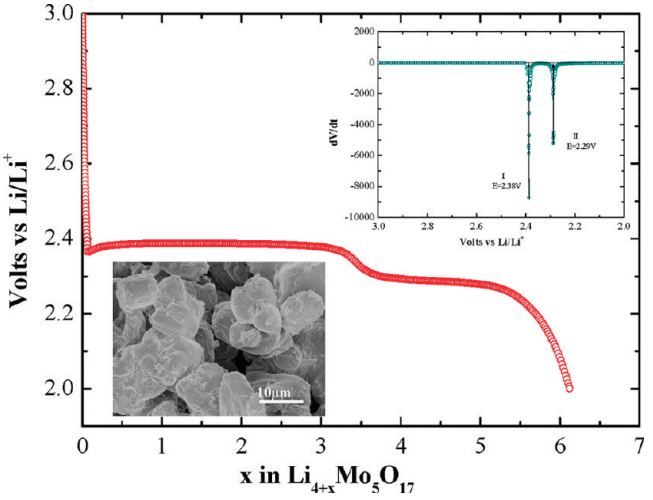

Figure 1. Voltage vs composition curve for the first discharge for $Li_4Mo_5O_{17}$ at a C/50 rate to 2.0 V. Inset: corresponding derivative curve dV/dt versus Li/Li^+ and SEM image of the parent phase $Li_4Mo_5O_{17}$.

Structural and Chemical Characterizations. The compounds were characterized by X-ray powder diffraction (XRD) using a Bruker D8 diffractometer with a capillary sample geometry and a Philips X'Pert diffractometer with Bragg−Brentano geometry (Cu $K\alpha_{1,2}$ radiation). Note that because of their instability in air, the XRD patterns of the reduced phases $Li_{4+x}Mo_5O_{17}$ were registered under vacuum using a chamber attached to the XRD instrument Philips. The electron diffraction (ED) studies were carried out on a JEOL 200CX electron microscope fitted with an eucentric goniometer (±60°) equipped with an EDS (energy dispersive spectroscopy) analyzer at room temperature. For the transmission electron microscopy study, the samples were crushed in *n*-butanol and deposited on a holey carbon membrane supported by a copper grid. The ED patterns were calculated with the JEMS v3.3708U2009 software. A scanning electron microscope (SEM) ZEISS SUPRA 55 was used for morphology studies. The lithium content was determined by atomic absorption spectroscopy with a Varian Spectra AA-20 instrument. Thermogravimetric analysis (TGA) was performed in N_2 atmosphere at a heating rate of 3 °C/min with a TG92 Setaram microbalance.

Results and Discussion

Electrochemical and Chemical Intercalation of Lithium in $Li_4Mo_5O_{17}$: Synthesis of $Li_{12}Mo_5O_{17}$. The electrochemical intercalation of lithium into $Li_4Mo_5O_{17}$ was performed at a rate of C/50, discharging the cell down to 2.0 V. The corresponding galvanostatic discharge curve (Figure 1) shows that six lithium ions can be inserted per

(18) Wiesmann, M.; Heitzel, H.; Svoboda, I.; Fuess, H. *Z. Kristallogr.* **1997**, *212*, 795.
(19) Brower, W. S.; Parker, H. S.; Roth, R. S.; Waring, J. L. *J. Cryst. Growth* **1972**, *16*, 115.
(20) Gatehouse, B. M.; Miskin, B. M. *J. Solid State Chem.* **1974**, *9*, 247.
(21) Gatehouse, B. M.; Miskin, B. M. *J. Solid State Chem.* **1975**, *15*, 274.
(22) Smit, J. P.; Stair, P. C.; Poppelmeier, K. R. *Cryst. Growth Des.* **2007**, *7*, 521.
(23) Pralong, V.; Delahaye-Vidal, A.; Chabre, Y.; Tarascon, J. M. *J. Solid State Chem.* **2001**, *162*, 270.
(24) Pralong, V.; Delahaye-Vidal, A.; Beaudoin, B.; Leriche, J. B.; Scoyer, J.; Tarascon, J. M. *J. Electrochem. Soc.* **2000**, *147*, 2096.

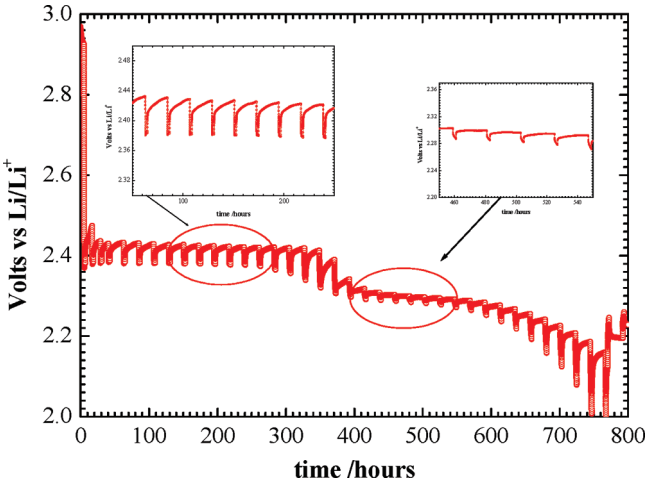

Figure 2. Chrono-potentiogram of $Li_4Mo_5O_{17}$ performed in a galvanostatic intermittent mode (GITT) with a rate of C/50 for 2 h and relaxation period of 30 min. Inset: enlargement showing the equilibrium potential of the reaction.

formula leading to the composition $Li_{10}Mo_5O_{17}$. Importantly, one observes two plateaus at 2.38 and 2.29 V, respectively, associated with sharp peaks on the derivative curve (inset, Figure 1). Such well-defined plateaus suggest the occurrence of biphasic processes with possibly the generation of a new structure for the fully reduced phase. To have a better insight into the biphasic process, we performed a galvanostatic intermittent titration (GITT, Figure 2) allowing access to the equilibrium potential in the course of the reduction. The two plateaus are related to two different structural changes due to the fact that the redox equilibrium potentials are different: 2.42 V and 2.30 V, respectively. From this low rate experiment, two compositions could be stabilized: $Li_8Mo_5O_{17}$ and $Li_{11}Mo_5O_{17}$ on the first and second plateaus, respectively. We observe that the lithium insertion is of course directly proportional to the kinetics used and a very low rate is required to insert a maximum of lithium, leading to the compound $Li_{11}Mo_5O_{17}$ with a rate of C/100. Note that these compounds correspond to a molybdenum mixed valence, $Mo^{4.6+}$ and $Mo^{5.2+}$, respectively, suggesting that the number of cations and their positions in the structure are the key parameters to stabilize the structure. In Figure 3 are reported the ex situ XRD patterns in the course of the first reduction. On the XRD pattern taken after the insertion of 1.7 Li/f.u., that is, in the middle of the first plateau (2.38 V), one can clearly observe the presence of the parent phase $Li_4Mo_5O_{17}$ reflections and the appearance of new reflections. At the end of the first plateau, 2.35 V, corresponding to the insertion of 4 Li/f.u., the pattern shows only the reflections of the new phase. Curiously, very few changes are observable after the further insertion of 3 Li/f.u. (2.0 V). This suggests that the insertion of additional lithium does not disrupt the so formed structure. In fact, the electrochemical synthesis has a very low kinetic, suggesting that a very long time, using for example, C/200, would be necessary to prepare the fully intercalated compound. To check this point, a chemical

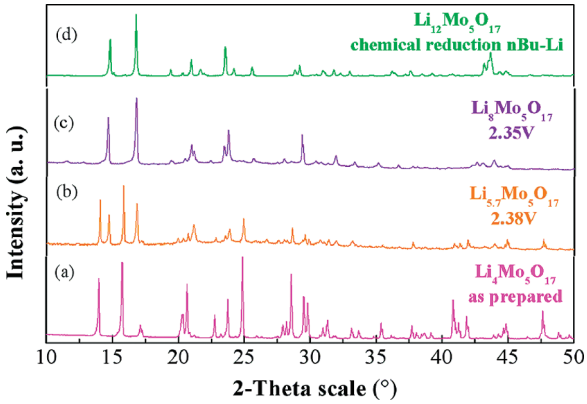

Figure 3. Powder X-ray diffraction patterns of (a) pristine $Li_4Mo_5O_{17}$, electrochemically discharged phase at (b) 2.38 V and (c) 2.35 V, and (d) reduced phase from the chemical reduction.

Table 1. Crystallographic Data for $Li_xMo_5O_{17}$, $x = 4$ [18] and $x = 12$

	$Li_4Mo_5O_{17}$ [ref 18]	$Li_{12}Mo_5O_{17}$ chemical reduction
space group	$P\bar{1}$	$P\bar{1}$
a (Å)	6.777(3)	6.547(1)
b (Å)	9.461(3)	8.848(1)
c (Å)	10.802(4)	11.601(1)
α (deg)	73.16(2)	77.431(3)
β (deg)	88.98(3)	96.295(3)
γ (deg)	69.76(3)	71.970(3)
cell volume (Å^3)	619.38	612.29(4)
χ^2		6.53
R_B (%)		8.81
R_{wp} (%)		6.00

reduction was performed in an argon filled glovebox to avoid the activity loss of *n*Bu-Li and for safety reasons, using 200 mg of $Li_4Mo_5O_{17}$ in 10 mL of a solution of anhydrous hexane, and 2.5 M *n*-buthyl lithium (*n*Bu-Li) in hexane was slowly added in excess (5 times) into solution with a single use 10 mL syringe. The resulted solution was stirred at room temperature for 3 days (eq. −2.0 V vs ENH). In these conditions, the atomic absorption analysis indicates that insertion reaches 12 Li/f.u. The XRD pattern of $Li_{12}Mo_5O_{17}$ (Figure 3d) is close to that obtained for $Li_{11}Mo_5O_{17}$ from electrochemical reduction but is better crystallized. Moreover, it appears that the $Li_{12}Mo_5O_{17}$ phase is more pure than the $Li_{11}Mo_5O_{17}$ phase, which may still contain a small fraction of the intermediate phase $Li_8Mo_5O_{17}$. In any case, the presence of amorphous carbon and the small thickness of the samples obtained by electrochemical intercalation do not allow a detailed structural analysis to be performed with accuracy.

Structural Study of $Li_{12}Mo_5O_{17}$. Bearing in mind that the electrochemical intercalation produces samples that contain amorphous carbon and that their corresponding phases are less well crystallized, the structural study was made only on the end member $Li_{12}Mo_5O_{17}$ prepared by *n*Bu-Li reduction. The structure resolution was performed using two XRPD patterns collected respectively on a D8 diffractometer with λ Cu Kα_1 radiation and an X'Pert Philips diffractometer with Cu K$\alpha_{1,2}$. The first one

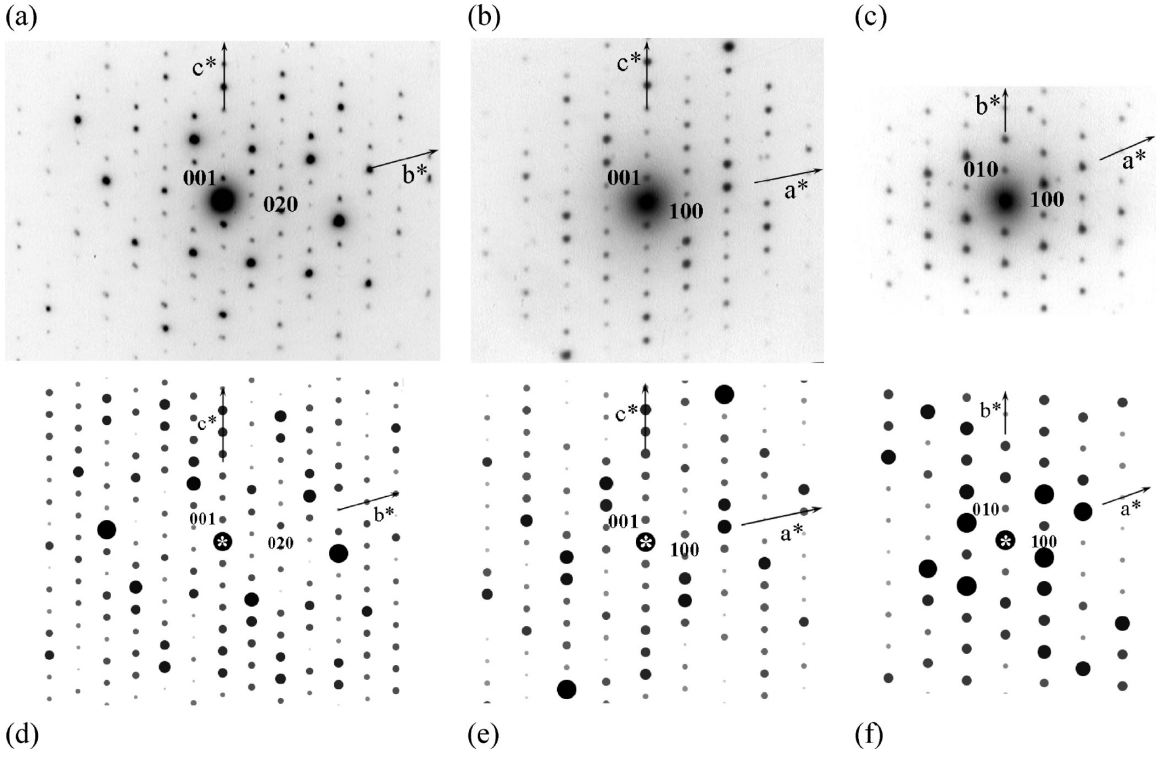

Figure 4. ED patterns recorded at room temperature along (a) [100], (b) [010], and (c) [001]. Calculated ED patterns with the structural model determined from XRPD along (d) [100], (e) [010], and (f) [001].

was used to index the first 20 reflections with the auto-indexing software DICVOL4.[25] This program gave a unique triclinic solution with high figures of merit $M(20) = 57.7$[26] and $F(20) = 103.1$.[27] The cell parameters of $Li_{12}Mo_5O_{17}$ exhibit a significant difference from those of $Li_4Mo_5O_{17}$ (Table 1) as expected from the very large difference in the patterns of these two compounds (Figure 3), but the similar cell volume suggests a strong relationship between the two structures. This triclinic cell was confirmed by electron diffraction, by tilting around the crystallographic axes, as shown from the ED patterns registered along [100] (Figure 4a), [010] (Figure 4b), and [001] (Figure 4c). The second XRPD pattern, registered in reflection geometry, was used to find the positions of the heaviest atoms, that is, the molybdenum and oxygen atoms. The positions of these atoms were determined from ab initio structure calculation, using the FOX program[28,29], supposing that such a structure involves, like $Li_4Mo_5O_{17}$, only MoO_6 octahedra. The structural model was built up with 5 MoO_6 octahedra, and we used the dynamical occupancy feature, implemented in FOX, to take into account oxygen atoms shared between building blocks. A structure solution was found with $[Mo_5O_{17}]_\infty$ ribbons of edge sharing MoO_6 octahedra running along the *b* axis, as in the parent structure $Li_4Mo_5O_{17}$. The Rietveld refinement of the oxygen and molybdenum atoms positions, performed with Fullprof, [30] yields to the following goodness of fit values: $R_{wp} = 6.73\%$, $R_B = 10.1\%$, and $\chi^2 = 8.29$. To find the lithium positions, we decided to use the empirical bond-valence rule as it was previously used as a tool for the prediction of crystal structures.[31] Bond valence calculations are included in the FOX program and can be used as a cost function to optimize the valence of the elements. Twelve Li sites were then added at random in the unit cell, while positional parameters were kept fixed for the Mo_5O_{17} framework. A structure solution was found where all the Li^+ cations have an octahedral coordination with a calculated valence close to +1. The final model possesses 102 positional parameters of which 36 are for the Li sites. It is worth mentioning that the Li has a too weak scattering factor to be refined by X-ray diffraction in such a complex structure and with strong X-ray scatterers. It is then unrealistic to perform a Rietveld refinement of Li positions without constraints with our X-ray data. Nevertheless, we have added 72 soft constraints on the Li−O distances to maintain the Li in positions where the calculated valence is close to one. The Rietveld refinement of this model, with soft constraints on Li−O distances, yields to small improvement in the goodness of fit values: $R_{wp} = 6.00\%$, $R_B = 8.81\%$, and $\chi^2 = 6.53$. The atomic coordinates are given in Table 2, and the final Rietveld plot is shown in Figure 5. This structural model determined from the XRD was used for the calculation of the ED patterns of the basal planes represented on Figure 4d−f. The variation of the intensity of the spots observed on the experimental ED patterns (Figure 4a−c) is similar to the one observed on the

(25) Boultif, A.; Louer, D. *J. Appl. Crystallogr.* **1991**, *24*, 987.
(26) De Wolff, P. M. *J. Appl. Crystallogr.* **1968**, *5*, 108.
(27) Smith, G. S.; Snyder, R. L. *J. Appl. Crystallogr.* **1979**, *12*, 60.
(28) Favre-Nicolin, V.; Cerny, R. *J. Appl. Crystallogr.* **2002**, *35*, 734.
(29) Cerny, R.; Favre-Nicolin, V. *Powder Diffraction* **2005**, *20*, 359.
(30) Rodriguez-Carvajal, J. *Physica B* **1993**, *192*, 55.
(31) Pannetier, J.; Bassas-Alsina, J.; Rodriguez-Carvajal, J.; Caignaert, V. *Nature* **1990**, *346*, 343.

Table 2. Atomic coordinates of molybdenum, lithium and oxygen in $Li_{12}Mo_5O_{17}$. The overall thermal factor is refined to $B_{iso} = 0.65(4)$ Å^2

atom	*x*/*a*	*y*/*b*	*z*/*c*
Mo1	0.1795(17)	0.7679(11)	0.7026(9)
Mo2	0.2365(18)	0.4619(13)	0.8347(10)
Mo3	0.2528(18)	0.9259(12)	0.3468(9)
Mo4	0.6335(15)	0.1945(12)	0.8866(8)
Mo5	0.7085(20)	0.3480(13)	0.5301(10)
Li1	0.54(3)	0.82(2)	0.579(19)
Li2	0.92(3)	0.60(2)	0.608(16)
Li3	0.01(4)	0.24(2)	0.75(2)
Li4	0.40(4)	0.99(3)	0.78(2)
Li5	0.29(4)	0.12(3)	0.99(2)
Li6	0.13(3)	0.11(2)	0.54(2)
Li7	0.34(3)	0.32(2)	0.631(17)
Li8	0.60(4)	0.51(3)	0.72(2)
Li9	0.81(3)	0.72(2)	0.814(17)
Li10	0.52(4)	0.36(2)	0.069(18)
Li11	0.94(4)	0.07(2)	0.105(20)
Li12	0.87(4)	0.41(2)	0.962(19)
O1	0.483(10)	0.744(7)	0.754(6)
O2	0.141(10)	0.699(6)	0.865(4)
O3	0.263(11)	0.560(8)	0.659(6)
O4	0.852(9)	0.839(6)	0.642(5)
O5	0.199(11)	0.869(7)	0.518(7)
O6	0.080(11)	−0.007(8)	0.713(6)
O7	0.207(12)	0.361(7)	1.003(6)
O8	0.546(11)	0.422(7)	0.891(6)
O9	0.927(12)	0.478(8)	0.790(6)
O10	0.339(10)	0.223(7)	0.815(5)
O11	0.533(10)	0.930(7)	0.395(6)
O12	0.330(9)	0.731(5)	0.287(4)
O13	0.272(11)	0.027(6)	0.166(6)
O14	0.954(10)	0.169(7)	0.927(5)
O15	0.606(11)	0.122(7)	0.039(6)
O16	0.010(10)	0.353(6)	0.570(5)
O17	0.386(11)	0.423(7)	0.459(6)

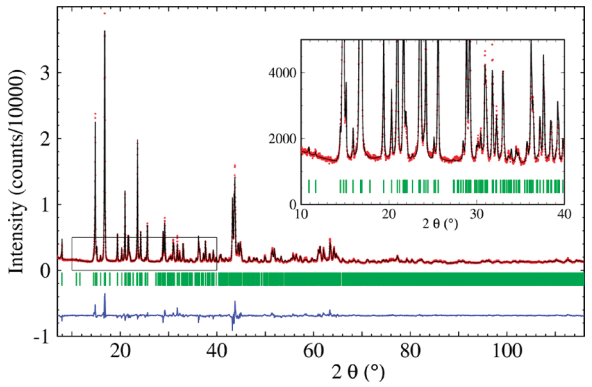

Figure 5. Rietveld refinement plot of $Li_{12}Mo_5O_{17}$: observed X-ray diffraction intensity (○) and calculated curve (line). The bottom curve is the difference of patterns, $y_{obs} - y_{cal}$, and the small bars indicate the angular positions of the allowed Bragg reflections.

calculated patterns (Figure 4d−f), which confirms the validity of the structural model.

The view of the structure of $Li_4Mo_5O_{17}$ (Figure 6a) and of $Li_{12}Mo_5O_{17}$ (Figure 6b) along the *a* axis shows that the lithium intercalation, as expected, does not change the arrangement of the MoO_6 octahedra. In both oxides the structure consists of $[Mo_5O_{17}]_\infty$ ribbons of edge sharing MoO_6 octahedra running along the *b* direction. In each ribbon, units of 2×3 edge-shared octahedral share edges with units of 2×2 edge-shared octahedra. Importantly, the geometry of the MoO_6 octahedra is different in

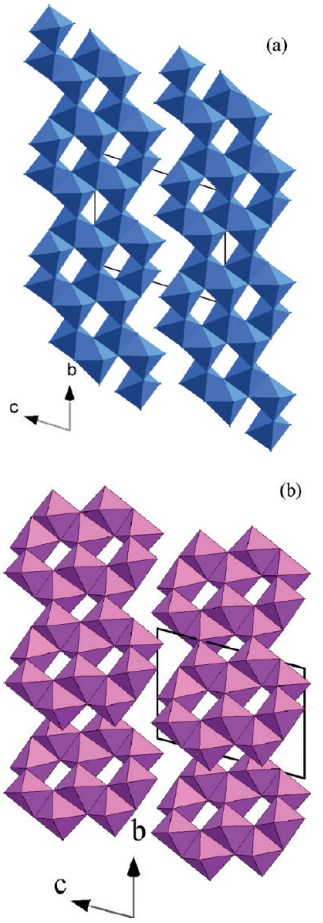

Figure 6. Comparison of the structural view along the *a* axis of $Li_4Mo_5O_{17}$ and $Li_{12}Mo_5O_{17}$. For clarity reasons, only the MoO_6 octahedra are represented to emphasize the relationship between the ribbon type structure $Li_4Mo_5O_{17}$ and reduced phase $Li_{12}Mo_5O_{17}$.

the two structures, as shown from the comparison of Mo−O interatomic distances in $Li_4Mo_5O_{17}$[18] and $Li_{12}Mo_5O_{17}$ (Table 3). One indeed observes that the MoO_6 octahedra are much more regular in $Li_{12}Mo_5O_{17}$, with Mo−O distances ranging from 1.79 Å to 2.22 Å, than those previously observed for $Li_4Mo_5O_{17}$ [18] whose distances are comprised between 1.70 Å and 2.49 Å. Such a higher symmetry of the octahedra in $Li_{12}Mo_5O_{17}$ is easily explained by the reduction of Mo^{6+} to $Mo^{4.4+}$, due to the intercalation. As a consequence, the geometry of the $[Mo_5O_{17}]_\infty$ ribbons is changed, that is, they are longitudinally compressed and transversally expanded in $Li_{12}Mo_5O_{17}$ compared to $Li_4Mo_5O_{17}$, explaining the decrease of the *b* parameter and the increase of the *c* parameter during lithium intercalation. Thus, the intercalation of lithium in $Li_4Mo_5O_{17}$ induces a topotactic antidistortion of the ribbon configuration, making the MoO_6 octahedra more symmetric. Note also, that the average Mo−O distances of the MoO_6 octahedra are longer in $Li_{12}Mo_5O_{17}$ than in $Li_4Mo_5O_{17}$, in agreement with the decrease of the oxidation state of molybdenum.

The relative positions of the $[Mo_5O_{17}]_\infty$ ribbons have not changed significantly as shown from Figure 5, except that they have been brought closer along *a* by lithium intercalation (Figure 7), leading to a decrease of the

Table 3. Selected Distances Mo−O for $Li_4Mo_5O_{17}$[18] and $Li_{12}Mo_5O_{17}$ [This Work]

$Li_4Mo_5O_{17}$			$Li_{12}Mo_5O_{17}$		
Mo1	O4	1.698(2)	Mo1	O1	1.94(7)
	O1	1.752(2)		O2	1.92(5)
	O13	1.895(2)		O3	1.94(7)
	O3	1.909(2)		O4	2.03(6)
	O7	2.139(2)		O5	2.17(8)
	O1	2.493(1)		O6	1.93(7)
⟨Mo−O⟩		**1.98**			**1.99**
			⟨Mo−O⟩		
Mo2	O6	1.699(2)	Mo2	O2	2.11(5)
	O5	1.762(2)		O3	2.08(7)
	O15	1.860(2)		O7	2.02(7)
	O7	1.965(2)		O8	1.96(7)
	O13	2.096(2)		O9	1.99(8)
	O11	2.474(2)		O10	2.08(6)
		1.98			**2.04**
Mo3	O10	1.716(2)	Mo3	O4	2.02(5)
	O11	1.752(2)		O5	2.04(8)
	O2	1.827(2)		O6	2.06(7)
	O7	2.000(2)		O11	1.87(7)
	O3	2.118(2)		O12	1.94(5)
	O5	2.435(2)		O13	2.13(7)
⟨Mo−O⟩		**1.98**			**2.01**
			⟨Mo−O⟩		
Mo4	O8	1.715(2)	Mo4	O8	1.93(6)
	O17	1.739(2)		O10	1.93(6)
	O14	1.822(2)		O12	2.04(5)
	O15	2.066(2)		O13	2.11(6)
	O13	2.210(2)		O14	2.03(7)
	O16	2.341(2)		O15	1.79(7)
⟨Mo−O⟩		**1.98**			**1.97**
			⟨Mo−O⟩		
Mo5	O9	1.736(2)	Mo5	O3	2.22(7)
	O12	1.751(2)		O5	2.05(7)
	O16	1.788(2)		O12	2.15(5)
	O3	2.124(2)		O16	1.99(7)
	O2	2.175(2)		O17	2.02(7)
	O14	2.208(2)		O17	1.96(6)
		1.96			**2.07**

a parameter for $Li_{12}Mo_5O_{17}$ compared to $Li_4Mo_5O_{17}$. As a consequence, the smaller cell volume of $Li_{12}Mo_5O_{17}$ ($V = 612$ Å^3) compared to $Li_4Mo_5O_{17}$ ($V = 619$ Å^3) is not due to the decrease of the size of the MoO_6 octahedra but to the electroattractive character of Li^+ cations which bring the ribbons closer to each other.

At this point, it is of great interest to consider the sites that may be available for Li^+ cations in this new structure. It should be noted that the single crystal study of $Li_4Mo_5O_{17}$[18] shows one Li in an octahedral coordination, while the three others have a tetrahedral coordination. However, it is of course not possible to determine the lithium positions from XRPD data in $Li_{12}Mo_5O_{17}$. Using bond valence calculations as a tool to locate positions of Li, we have been able to suggest 12 possible sites for lithium. These Li sites all exhibit an octahedral coordination, and the view of the "hypothetical" structure $Li_{12}Mo_5O_{17}$ along *c* (Figure 8) shows that it can be described as a distorted rock salt type structure involving an ordering between LiO_6 and MoO_6 octahedra. A combined neutron diffraction and X-ray synchrotron study will be necessary to confirm this structure with accuracy.

Mobility of Lithium in $Li_4Mo_5O_{17}$. Curiously the ionic conductivity of $Li_4Mo_5O_{17}$ has never been explored to date to our knowledge. The impedance plots registered between 10 and 120 kHz for different temperatures (inset Figure 9a) show that this oxide is a cationic conductor, since a semi-circle is observed at high frequency, followed by a spike in the low frequency region. The ionic conductivity increases with temperature, reaching $\sim 10^{-3.5}$ S·cm^{-1} at 500 °C. The plot of $\log(\sigma)$ versus $1000/T$ (Figure 9a) shows a linear feature, obeying the classical Arrhenius relation $\ln(\sigma T) = \ln(\sigma_o) - E_a/k_BT$. It proves only one regime of conductivity characterized by an activation energy $E_a = 0.35$ eV. The conductivity is in the same range as other lithium ions conductors[32] like the rock salt Li_2TiMgO_4[33]

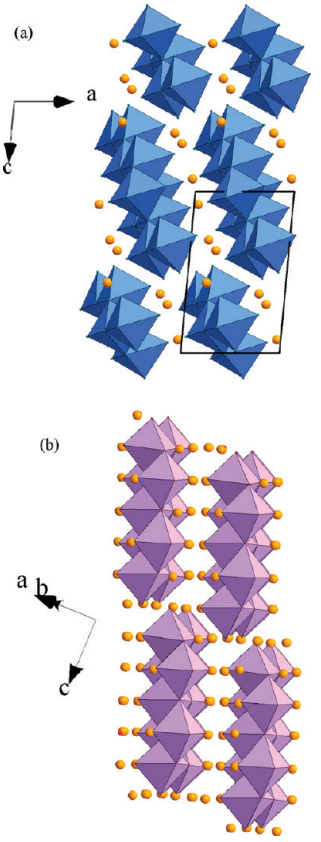

Figure 7. Comparison between the two structures of $Li_4Mo_5O_{17}$ and $Li_{12}Mo_5O_{17}$, along [010] and (−5, 12, 6), respectively, showing the lithium cations surrounding the $[Mo_5O_{17}]_\infty$ ribbons.

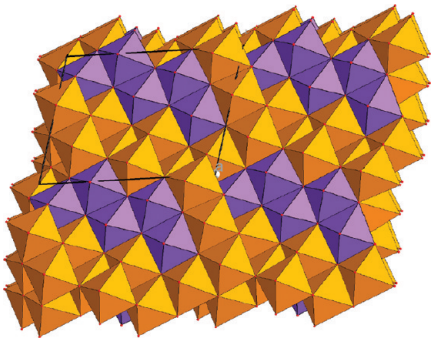

Figure 8. Representation of the $Li_{12}Mo_5O_{17}$ structure along the *c* axis, showing the rock salt type arrangement of the MoO_6 and LiO_6 octahedra.

(32) Knauth, P. *Solid State Ionics* **2009**, *180*(14−16), 911–916.
(33) Kishore, M. S.; Marinel, S.; Pralong, V.; Caignaert, V.; D'Astorg, S.; Raveau, B. *Mater. Res. Bull.* **2006**, *41*, 1378.

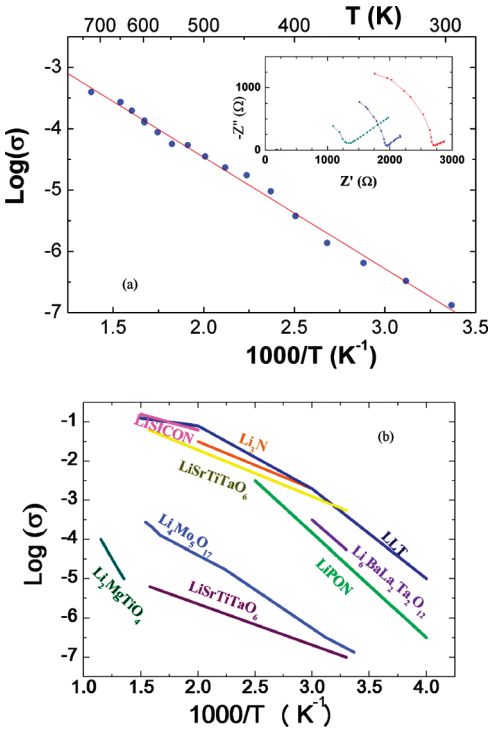

Figure 9. (a) Arrhenius plot log(σ) versus $1/T$ of $Li_4Mo_5O_{17}$ under air. Inset: Nyquist plots at 30 °C. (b) Arrhenius plots of the lithium ion conductivities (bulk) of selected metal oxides.

Table 4. Comparison of the Lithium Ionic Conductivity and Activation Energy Values for Li-Ion Conductors Reported in the Literature

formula	temperature range (K)	σ (S/cm)	E_a (eV)	references
Li_3N	300−500	$10^{-2.7}$−$10^{-1.5}$		36
lipon	250−400	$10^{-6.5}$−$10^{-2.5}$	0.45	36
$Li_{2.9}Si_{0.45}PO_{1.6}N_{1.3}$				
lisicon	300−700	10^{-6}−$10^{-0.8}$	0.4−0.6	36, 37
$Li_{14}ZnGe_4O_{16}$				
$LiSrTiTaO_6$	300−640	$10^{-3.26}$−$10^{-1.2}$		34
$Li_6BaLa_2Ta_2O_{12}$	300−340	$10^{-4.26}$−$10^{-3.5}$	0.4−0.6	35
rock salt	300−600	10^{-3}−$10^{-1.5}$	0.37−0.45	37, 40
$Li_3Ni_3NbO_6$				
rock salt	700−900	10^{-4}−$10^{-2.5}$	0.53	33
Li_2MgTiO_4				
lamellar	300−770	$10^{-5.23}$−$10^{-1.77}$	0.41	38
$Na_{0.8}Co_{0.4}Ti_{0.6}O_2$				
LLT	300−400	$10^{-3.3}$−$10^{-2.22}$	0.31	39, 41
$LaLi_{0.8}Ti_2O_6$				
$Li_4Mo_5O_{17}$	300−700	$10^{-6.8}$−$10^{-3.4}$	0.35	this work

and $LiSrTiTaO_6$ [34] but also about two orders of magnitude less than the best candidates such as the garnet $Li_5La_3Nb_2O_{12}$, $Li_6BaLa_2Ta_2O_{12}$, Li_3N, or the phase $Li_{0.34}La_{0.51}TiO_2$ (LLT) [32,35−41] (Figure 9b, Table 4). The conductivity of $Li_{12}Mo_5O_{17}$, could not be investigated because of its instability and rapid oxidation in air.

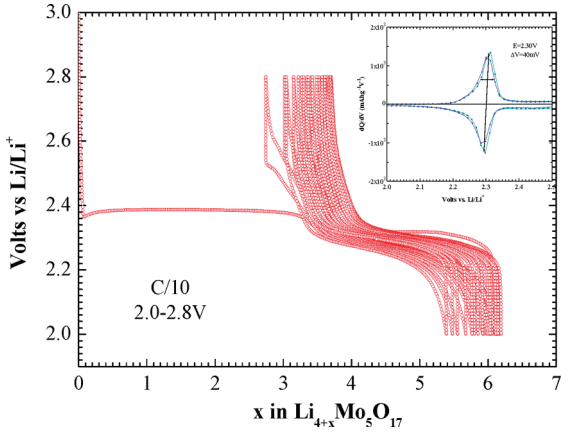

Figure 10. Potential versus capacity curve at C/10 in the 3−2 V potential window. Inset: corresponding incremental capacity dx/dV versus potential curve of the second cycle.

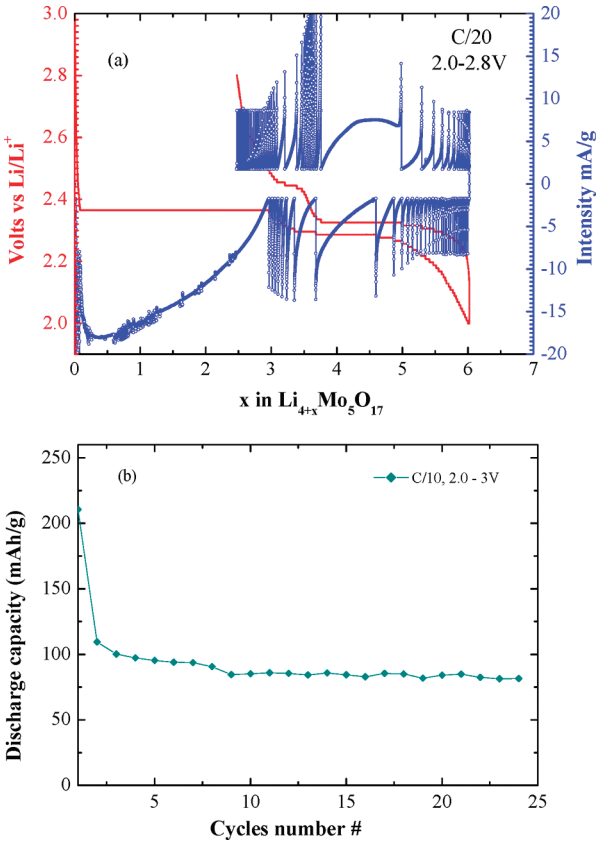

Figure 11. (a) Potentiometric titration curve (PITT) during the first cycle of $Li_4Mo_5O_{17}$ in the range of 3.0−2.0 V vs Li/Li^+ limitation of the 10 mV potential step in duration of 1 h and current limitation equivalent to a galvanic current $I_{limit} = I_{C/50}$. (b) Specific discharge capacity versus cycle number of $Li_4Mo_5O_{17}$. The potential window is 3−2.0 V, and the cycling rate is C/10.

Electrochemical Behavior of $Li_4Mo_5O_{17}$ and $Li_{12}Mo_5O_{17}$. The charge discharge profiles have been performed by a galvanostatic cycling at C/10 in the potential window 2.0−2.8 V versus Li/Li^+ (Figure 10). After the first cycle, a reversible capacity of 3 Li/f.u. (100 mA·h/g) is obtained on the second plateau at an average potential of 2.30 V.

(34) Thangadurai, V.; Weppner, W. *Ionics* **2002**, *8*, 281.
(35) Thangadurai, V.; Weppner, W. *Ionics* **2006**, *12*, 81.
(36) Sebastian, L.; Gopalakrishnan, J. *J. Mater. Chem.* **2003**, *13*, 433.
(37) Thangadurai, V.; Adams, S.; Weppner, W. *Chem. Mater.* **2004**, *16*, 2998.
(38) Bruce, P. J.; West, A. R. *J. Electrochem. Soc.* **1983**, *130*(3), 662.
(39) Shin, Y.-J.; Park, M.-H.; Kwak, J.-H.; Namgoong, H.; Hee Han, O. *Solid State Ionics* **2002**, *150*, 363.
(40) Mather, G. C.; West, A. R. *J. Solid State Chem.* **1996**, *124*, 214.
(41) Inaguma, Y; Liquan, C.; Itoh, M.; Nakamura, T.; Uchida, T.; Ikuta, H.; Wakihara, M. *Solid State Com.*, **1993**, *86*(10), 689–693. Zou, Y.; Inoue, N. *Ionics* **2005**, *11*, 333.

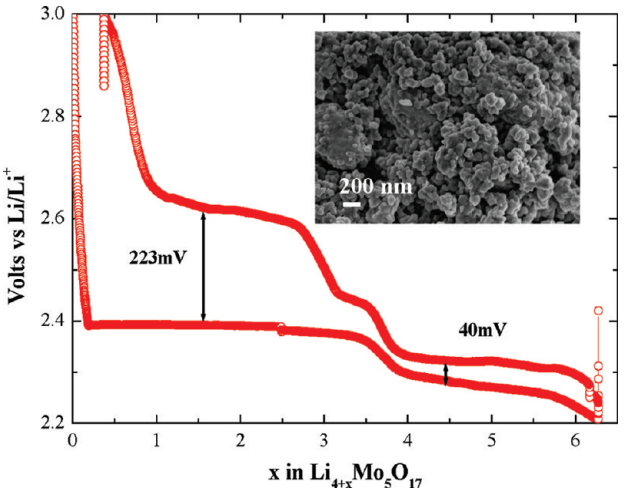

Figure 12. Potential versus capacity curve at C/100 in the 3−2 V potential window for $Li_4Mo_5O_{17}$ ball milled for 1 h with 20 wt % acetylene black. Inset: SEM image of the ball-milled $Li_4Mo_5O_{17}$ phase.

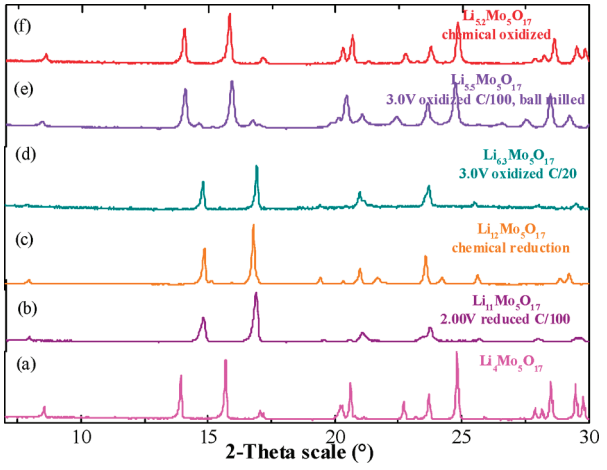

Figure 13. Powder X-ray diffraction patterns of (a) pristine $Li_4Mo_5O_{17}$, (b) electrochemically discharged phase $Li_{11}Mo_5O_{17}$, (c) chemically discharged phase $Li_{12}Mo_5O_{17}$, (d) electrochemically charged phase $Li_{6.3}Mo_5O_{17}$ 2.0 V (C/20), (e) electrochemically charged ball milled phase $Li_{5.5}Mo_5O_{17}$ 2.0 V (C/100), and (f) chemically charged phase $Li_{5.2}Mo_5O_{17}$.

As shown on the derivative curve (inset, Figure 10), the sharp redox peaks occurring at 2.30 V exhibit a low polarization of about 40 mV in cycling. The potentiodynamic titration curve (PITT, Figure 11a) reveals a bell shape type response on the reversible phenomena [23] and confirms together with the sharpness of the peaks in the derivative curve that the reversible process is biphasic. The plot of discharge capacity versus cycle number (Figure 11b) indicates a drop of capacity after the first cycle, followed by a stable reversible capacity of 100 mA·h/g even after 20 cycles for a C/10 rate.

A complete reduction of $Li_4Mo_5O_{17}$ to $Li_{12}Mo_5O_{17}$ and a complete reoxidation leading back to the parent phase is rather difficult and may be due to the large size of the particles. Indeed, as already mentioned above, a rate of C/100 is necessary to reach $Li_{11}Mo_5O_{17}$ upon reduction. Regarding the oxidation, a good reversibility is obtained on the second plateau, occurring at 2.29 V involving the phases $Li_8Mo_5O_{17}$ and $Li_{11}Mo_5O_{17}$. Nevertheless, the XRD patterns of the phases taken in the course of the reversible process on the second plateaus show very few differences (Figure 13), and further investigations with neutron diffraction are needed to have better insight into the structural transformation occurring between the composition $Li_8Mo_5O_{17}$ and $Li_{11}Mo_5O_{17}$. At this point, the issue of the complete reversibility of the process, that is, of the possible deintercalation from the rock salt structure $Li_{12}Mo_5O_{17}$ into the parent structure "$Li_4Mo_5O_{17}$", must be raised. To answer this question, we performed a chemical oxidation by adding 110 mg of NO_2BF_4 to 100 mg of the reduced phase (molar ratio 1:5) in 10 mL of acetonitrile under stirring at room temperature during 4 days. Such a strong oxidizing agent is currently used to simulate a potential of 2.1 V vs ENH. On Figure 13 is reported the XRD pattern obtained after 5 days of treatment at room temperature. One can easily observe that the parent structure is completely recovered; we performed a Rietveld refinement on the XRPD data with the structural model of "Li_4" and found the following cell parameters: $a = 6.753(1)$ Å, $b = 9.499(1)$ Å, $c = 10.819(1)$ Å, $\alpha = 72.89°$, $\beta = 96.3°$, $\gamma = 69.72°$, and a volume $V = 619.97$ Å^3. In addition, the atomic absorption analysis gives a composition close to $Li_{5.2\pm0.1}Mo_5O_{17}$, suggesting a tolerance of the "Li_4" structure to accommodate a few additional lithium ions without any structural changes. This information, combined with the fact that the intermediate composition $Li_8Mo_5O_{17}$ does exist from the electrochemical curve, suggests that all 12 lithium sites are not equivalent and that, at least, for four of them the extraction may be very difficult, requiring extreme experimental conditions for the reversibility. One could also suggest that reducing the particle size to the nanoscale should allow removing all the lithium, so that way the theoretical capacity of 270 mA·h/g (8 Li/f.u.) could be reached. As shown on Figure 12, a complete reversibility is obtained by electrochemistry when the active material is ball milled for 1 h with 20 wt % acetylene black. Note that a large polarization of about 242 mV is observed on the first plateau, (compared to only 40 mV polarization on the second plateau). Such a process allowed us to decrease the particle size to 100 nm as shown from the SEM image inset in Figure 12. The corresponding XRD pattern (Figure 13) is comparable to the one obtained by chemical oxidation. Thus, we prove the complete reversibility of the structural transformation. Preparing this phase at the nanoscale will thus reduce the lithium path length and decrease the large polarization occurring in the course of the structural transformation.

Conclusion

The intercalation of lithium in a lithium molybdate with a ribbon structure has been achieved for the first time. This result demonstrates that the great flexibility of

the ribbons allows substantial amount of lithium to be intercalated and opens the route to the exploration of other molybdates, whose structure consists of ribbons or layers of molybdenum polyhedra. This topotactic and reversible transformation of $Li_4Mo_5O_{17}$ into $Li_{12}Mo_5O_{17}$ suggests strongly that lithium sits in octahedral sites of the so formed rock salt type "$\square_{12}Mo_5O_{17}$" framework. A combined neutron diffraction and X-ray synchrotron study will be necessary to solve this new structure with accuracy.

Acknowledgment. We gratefully acknowledge the CNRS and the Minister of Education and Research for financial support through their Research, Strategic, and Scholarship programs and the European Union for support through the network of excellence Novelox and FAME.